AN INTEGRAL EQUATION METHOD FOR SOLVING LAPLACE'S EQUATION WITH ROBIN BOUNDARY CONDITIONS

by

Todd Keeler

B.Sc. (Computational Science), University of Alberta, 2005

B.Sc. (Physics), University of Alberta, 2004

THESIS SUBMITTED IN PARTIAL FULFILLMENT

OF THE REQUIREMENTS FOR THE DEGREE OF

MASTER OF SCIENCE

IN THE

DEPARTMENT OF MATHEMATICS

FACULTY OF SCIENCE

SIMON FRASER UNIVERSITY

Fall 2011

APPROVAL

Name: Todd Keeler

Degree: Master of Science

Title of Thesis: An Integral Equation Method for Solving Laplace's Equation with Robin Boundary Conditions

Examining Committee:

Dr. David Muraki
Professor
(Chair)

Dr. Mary Catherine Kropinski
Associate Professor
(Senior supervisor)

Dr. John Stockie
Associate Professor
(Supervisor)

Dr. Nilima Nigam
Associate Professor
(Internal)

Date Approved: Dec 6, 2011

Declaration of
Partial Copyright Licence

Abstract

Boundary integral equations have been used to create effective methods for solving elliptic partial differential equations. Of primary importance is choosing the appropriate boundary representation for the solution such that the resulting integral equation is well-conditioned and solvable. Traditional boundary representations for Laplace's equation use a double layer potential for Dirichlet problems and a single layer potential for Neumann problems since both lead to Fredholm integral equations of the second kind with continuous kernels. We investigate a representation that gives rise to Fredholm equations of the second kind for Robin boundary conditions. The equations have singular kernels for which we use specialized quadrature rules to construct numerical approximations. We also study the solution and conditioning of these methods with weak Robin conditions that approach Dirichlet ones in the limit and for domains that are multiply connected.

To my wife Lauri and my sons Jacob, Liam, Camden, and Nathaniel

Acknowledgments

I would like to acknowledge and thank my supervisor, Dr. Mary Catherine Kropinski, for her long-suffering and support. In addition, I would like to thank my graduate committee and chair for their advice and support.

Contents

List of Tables

List of Figures

Chapter 1

Introduction

Boundary integral equations (BIEs) were initially used as tools to prove the existence of solutions to elliptic partial differential equations (PDEs) such as Laplace's equation with certain boundary conditions using Fredholm theory [3]. A more modern use of boundary integral equations is to approximate them with a suitable numerical quadrature rule, creating viable numerical methods for solving PDEs[1]. Of primary importance is choosing the appropriate boundary representation for the solution such that the resulting integral equation is well-conditioned and solvable. In this thesis we investigate a representation that gives rise to Fredholm equations of the second kind for Laplace's equation with Robin boundary conditions in two dimensions. The integral operators have singular kernels for which we use specialized quadrature rules. We also numerically study the solution and conditioning of these methods with Robin conditions that approach Dirichlet ones in the limit and for domains that are multiply connected.

The mathematical theory regarding Laplace's equation is often referred to as potential theory, given the significance the equation holds for describing physical phenomena such as gravitational and electrical potentials. In fact, our BIEs can be conceptualized as obtaining the solution of Laplace's equation represented as the electrical potential of a charge distribution on the boundary of the solution domain. Analysis of BIEs requires use of both Fredholm and potential theory and we provide a brief overview of both in Chapter two.

Chapter three will describe the numerical treatment of our method, focussing on Nyström's method and specialized quadrature rules for two dimensions. The chapter concludes with a review of a cur-

rent technique that could be used to implement a three dimensional version of our BIE formulation.

In Chapter four we present numerical results demonstrating high order convergence on some geometries for our formulation for exterior, interior and multiply connected domains. We also present results related to solving boundary conditions of the Robin type that approach a Dirichlet boundary condition in the limit. In this limit our BIE formulation becomes a Fredholm integral equation of the first kind with a singular kernel. Finally, we apply our singular quadrature methods directly to the Dirichlet problem, with results showing our method converges despite the fact that the condition number of the numerical scheme grows unbounded as the number of quadrature points increases.

Chapter 2

Potential theory and Boundary Integral Equations

The topic of this thesis is to construct high-order numerical solutions to BIEs associated with solving Laplace's equation in two and three dimensions. Specifically, we seek to approximate a function u on a finite bounded domain $\Omega \in \mathbb{R}^2$ with smooth boundaries Γ such that

$$\nabla^2 u(x) = 0, \qquad x \in \Omega, \tag{2.1}$$

$$\beta \partial_n u(y) + u(y) = g(y), \qquad y \in \Gamma. \tag{2.2}$$

$\beta > 0$ is a function on Γ and g is the boundary data. ∂_n refers to the outward normal derivative on Γ. For negative β, this problem is ill-posed, since solutions are not unique. For example, in $\mathbb{R}^2$ take $\beta = -1$ on the unit circle with $u(\hat{x}, \hat{y}) = \hat{x}$.

We also consider an exterior problem where we look for a solution in the unbounded domain Ω^c, with the following boundary condition

$$\nabla^2 u(x) = 0, \qquad x \in \Omega^c, \tag{2.3}$$

$$-\beta \partial_n u(y) + u(y) = g(y), \qquad y \in \Gamma. \tag{2.4}$$

In this exterior case, well-posedness requires at the negative sign in front of $\beta > 0$, keeping the normal consistent with the interior case. For the exterior problems, one must define conditions at ∞. In two dimensions we require that u is $O(1/r)$ as $r = |x| \to \infty$. For the 3d problem we require

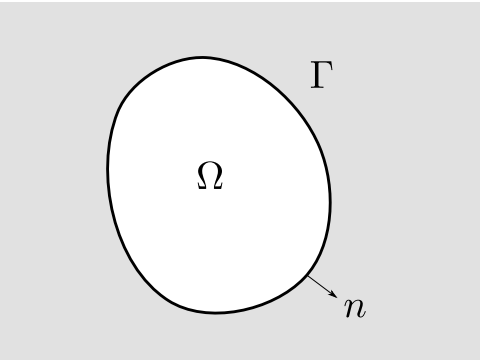

Figure 2.1: Interior and exterior domains.

that $u(x) \to 0$ as $|x| \to \infty$. Constanda in [5] shows that solutions to the above problems exist and are unique in 2d, with $\beta > 0$. Standard formulations of Robin boundary conditions, as in [5], often assign the coefficient β to u instead of $\partial_n u$. We use our formulation as we are interested in the limit $\beta \to 0$ at which point our formulation becomes a Dirichlet problem. Existence and uniqueness in 3d can be found in [6] for the interior problem. To find a solution to the Robin problem, we propose a boundary representation of u as a single layer potential $\sigma(y), y \in \Gamma$:

$$u(x) = \int_\Gamma \sigma(y) G(y,x) dS_y, \quad x \in \Omega. \tag{2.5}$$

Here $G(x,y)$ is the fundamental solution to Laplace's equation in $\mathbb{R}^{2,3}$, specifically:

$$G(x,y) = \frac{\log|x-y|}{2\pi}, \quad x,y \in \mathbb{R}^2. \tag{2.6}$$

$$G(x,y) = \frac{-1}{4\pi|x-y|}, \quad x,y \in \mathbb{R}^3. \tag{2.7}$$

While u represented in this fashion is by design harmonic in Ω for any σ, satisfying the boundary conditions leads to a Fredholm Integral equation of the second kind for σ for both the interior Robin problem

$$\beta(x)\left[-\sigma(x)/2 + \int_\Gamma \sigma(y)\partial_{n_x} G(y,x) dS_y\right] + \int_\Gamma \sigma(y) G(y,x) dS_y = g, \tag{2.8}$$

and the exterior Robin problem

$$-\beta(x)\left[\sigma(x)/2 + \int_\Gamma \sigma(y)\partial_{n_x} G(y,x) dS_y\right] + \int_\Gamma \sigma(y) G(y,x) dS_y = g. \tag{2.9}$$

We will also define a domain Ω_m that is bounded and multiply connected as in Figure 2.2. We will give some numerical results in this domain, including an unbounded version with Γ_0 removed.

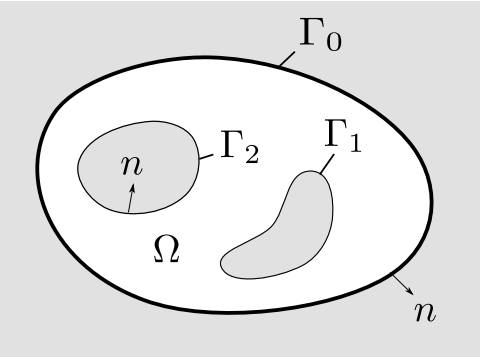

Figure 2.2: Bounded and multiply connected domain.

This chapter provides a theoretical overview for understanding these Boundary Integral Equations in the context of solving Laplace's equation.

2.1 The Laplacian: Greens Identities and the Fundamental Solution

The Laplacian ∇^2 is defined as the following partial differential operator on $\mathbb{R}^n$,

$$\nabla^2 f(x) = \sum_{i=1}^{n} \partial_i^2 f(x) \tag{2.10}$$

where $f(x)$ is a function mapping $x \in \mathbb{R}^n$ to $\mathbb{R}$, and has at least the requisite two partial derivatives. A function is said to be harmonic on a domain Ω if

$$\nabla^2 f(x) = 0,\ x \in \Omega. \tag{2.11}$$

For harmonic functions u, v, we have the following Green's identities,

$$\int_\Gamma v \partial_n u dS = \int_\Omega v \nabla^2 u + \nabla v \cdot \nabla u dV. \tag{2.12}$$

$$\int_\Gamma v \partial_n u - u \partial_n v dS = \int_\Omega v \nabla^2 u - u \nabla^2 v dV. \tag{2.13}$$

A fundamental solution $\Theta(x, y)$ of the Laplacian is one for which

$$\nabla^2\Theta(x, y) = \delta(x - y), \tag{2.14}$$

where δ is the Dirac delta function. (2.14) needs to be interpreted in a distributional sense. I.e. for infinitely smooth test functions ϕ with compact support in $\mathbb{R}^n$ we have

$$\int_{\mathbb{R}^n} \Theta\nabla^2\phi dV = \phi(0). \tag{2.15}$$

That $G(x, y)$ is the fundamental solution to Laplace's equation in $\mathbb{R}^{2,3}$ can be found in [7].

Given the fundamental solution to Laplace's equation in two and three dimensions, we can describe the solution to the inhomogeneous equation, with $\rho(x) \in C^2(\mathbb{R}^{2,3})$

$$\nabla^2 u(x) = \rho(x), \quad x \in \mathbb{R}^{2,3} \tag{2.16}$$

by the convolution,

$$u = G * \rho = \int_{\mathbb{R}^{2,3}} G(x, y)\rho(y)dS_y \tag{2.17}$$

subject to the condition in 2d that $\int_{\mathbb{R}^2} |\log(y)||\rho(y)|dS_y < \infty$. The solution to this equation has significant physical interpretation, though more so in three dimensions, as the electric or gravitational potential due to a charge distribution ρ.

The fundamental solution also allows us to represent the solution u to Laplace's equation solely by its boundary values. Substituting the fundamental solution into Green's second identity (2.13) gives

$$\int_\Gamma u(y)\partial_{n_y}G(x, y) - G(x, y)\partial_n u(y)dS_y = \int_\Omega u(y)\nabla_y^2 G(x, y) - G(x, y)\nabla^2 u(y)dV_y. \tag{2.18}$$

Since u is harmonic in Ω and by (2.15)

$$u(x) = \int_\Gamma u\partial_{n_y}G(x, y) - G(x, y)\partial_n u dS. \tag{2.19}$$

Equation (2.19) shows that in Ω, u can be described by the boundary integral of its normal derivative and value combined with the value and normal derivative of the fundamental solution. In the context of potential theory, we have described a potential u by a distribution of charge on the boundary. The fact that u can be represented in this fashion leads us to alternative boundary representations of the harmonic function u in terms of a distribution of charge density on the boundary. We will introduce these in the following section and show how one leads to our BIE's for solving Laplace's equation with Robin type boundary conditions.

2.2 Boundary Integral Equations

Instead of representing a harmonic function u by its boundary data and normal derivative as in (2.19), the following representations are used, for example, by Folland[7]:

$$u(x) = \int_\Gamma \sigma(y) G(y,x) dS_y. \tag{2.20}$$

$$u(x) = \int_\Gamma \sigma(y) \partial_{n_y} G(y,x) dS_y. \tag{2.21}$$

These boundary representations are called the single layer potential (2.20) and the double layer potential (2.20). The quantity $\sigma(y)$ is an unknown function on Γ called a density function. Folland [7] uses a double layer potential for problems with Dirichlet boundary conditions and the single layer potential for those with Neumann boundary conditions. In our case, are conditions are of a mixed type, and the purpose of this thesis is to study the result of resolving Robin boundary conditions using the single layer potential. The question remains, given boundary data for u, can one find the appropriate σ.

There are two distinct components to our boundary condition: the Dirichlet component describing the value of u on Γ and the Neumann component describing the normal derivative of u on Γ. For the Neumann condition, we will need to investigate the extension of the normal derivative of the single layer potential as it approaches Γ, as opposed to the extension of the layer potential itself for the Dirichlet problem. We will state the result of these extensions, Folland gives a rigorous treatment in [7].

The normal derivative of u on Γ when represented by (2.21) takes the following value on the boundary of the interior problem,

$$\partial_{n_x} u(x) = -\sigma(x_0)/2 + \int_\Gamma \sigma(y) \partial_{n_x} G(y,x) dS_y, \quad x, y \in \Gamma, \tag{2.22}$$

and the boundary of the exterior problem,

$$\partial_{n_x} u(x) = \sigma(x_0)/2 + \int_\Gamma \sigma(y) \partial_{n_x} G(y,x) dS_y, \quad x, y \in \Gamma. \tag{2.23}$$

The values are different, since the derivative of the single layer potential is not continuous in the normal direction on Γ. The extra terms $\pm\sigma/2$, called a jump condition, is important to our integral

equation formulation. These extra terms cause our equations to be Fredholm equations of the second kind.

The value of (2.20) is however continuous across the boundary.

$$u(x) = \int_\Gamma \sigma(y) G(y,x) dS_y, \quad x, y \in \Gamma. \tag{2.24}$$

Combining equations (2.22), (2.23), and (2.24) with the Robin boundary conditions (2.2) and (2.4)leads to the BIEs (2.8) and (2.9).

2.3 Fredholm Theory and Compact Operators

Fredholm theory gives a framework for determining the uniqueness and existence of solutions to equations of the form

$$B\sigma = (I + \lambda A)\sigma = g \tag{2.25}$$

where I is the identity operator, λ a constant parameter and A is a compact operator. Atkinson[3] offers the following definition for compact operators:

Definition 1. *Let X and Y be normed vector spaces, and let $A : X \to Y$ be linear. Then A is compact if for every bounded sequence $x_n \subset X$, the sequence Ax_n has a subsequence that is convergent to some point in Y.*

We will consider integral operators that map $L^2(\Gamma) \to L^2(\Gamma)$ of the form

$$A\sigma = \int_\Gamma \mathbb{K}(x,y)\sigma(y) dS_y. \tag{2.26}$$

Integral operators of this form are compact if the kernel $\mathbb{K}$ is in $L^2(\Gamma \times \Gamma)$. Or in other words if

$$\int_\Gamma \int_\Gamma |\mathbb{K}(x,y)|^2 dS_x dS_y < \infty. \tag{2.27}$$

$$\int_\Gamma |\mathbb{K}(x,y)|^2 dS_y < \infty. \; \forall x \in \Gamma. \tag{2.28}$$

$$\int_\Gamma |\mathbb{K}(x,y)|^2 dS_x < \infty. \; \forall y \in \Gamma. \tag{2.29}$$

The primary statement of Fredholm theory is the Fredholm Alternative [8] which states, as applied to our operators above:

- either $(I+\lambda A)\sigma = 0$ has only the trivial solution and the solution to $(I+\lambda A)\sigma = f \in L^2(\Gamma)$ exists and is unique for all f.
- or $(I + \lambda A)\sigma = 0$ has a non-trivial solution and $(I + \lambda A)\sigma = f$ exists only if f is in the range of $I + \lambda A$. In this case σ is non-unique, since adding any non-trivial element of the null-space of $I + \lambda A$ to σ will still be a solution.

The usefulness of this theory is that it reduces the question of uniqueness and existence of solutions of $B\sigma = f$ to analyzing the null space of B. Folland uses boundary integral equations and Fredholm theory in this manner to provide proof for the existence and uniqueness of solutions to Laplace's equation with Dirichlet and Neumann boundary conditions.

In our case, the kernels of our integral operators are compact. For $\beta > 0$ we have Fredholm equations of the second kind that are subject to the Fredholm Alternative. Though we don't give a formal proof as to the existence and uniqueness for solutions to our BIE's, our numerical results provide evidences that a solution exists and is unique, at least for our test geometries.

Proof to the existence of solutions for the following problem in $\mathbb{R}^3$ is given in Kellogs 'Foundations of Potential Theory'[6] using the Fredholm alternative,

$$\sigma(x)/2 + \int_\Gamma \sigma(x)\partial_{n_x} G(x,y)dS_y + h(x)\int_\Gamma \sigma(x)G(x,y)dS_y = g. \tag{2.30}$$

for $h > 0$. Dividing (2.8) by constant β gives the same form as (2.30) and thus we expect the 3d interior Robin problem to have unique solutions that exist for any g.

Constanda in [5] uses the Fredholm alternative to prove existence to solutions of Laplaces equation in 2 dimensions for Dirichlet, Robin and Neumann problems for continuous boundary data. An important aspect of solving 2d integral equations for the Robin problem is that there exists boundaries that allow nontrivial solutions to

$$\int_\Gamma \sigma(y)\log(|y-x|)dS_y = 0 \quad x \in \Gamma. \tag{2.31}$$

We have the following theorem from Constanda,[5] who also gives its proof:

Theorem 1. *For every simple closed* Γ *and any* $\alpha \in (0,1]$*, there is a unique non-zero function* $\Phi \in C^{0,\alpha}(\Gamma)$ *and unique constant* w *such that*

$$-\int_\Gamma \frac{\log(x-y)}{2\pi}\Phi(y)dS_y = w, \quad \int_\Gamma \Phi(y)dS_y = 1. \tag{2.32}$$

$C^{0,\alpha}$ is the space of Holder continuous functions on Γ with index α. The value $e^{2\pi w}$ is known as the logarithmic capacity of Γ. For logarithmic capacity of one, $w = 0$ and non-trivial null solutions exist for 2.31. We call a boundary for which $w = 0$ holds a pathological boundary.

For pathological boundaries, we suspect that our 2d formulation for the Robin problem will contain a non-trivial homogeneous solution. However, one can avoid these contours, according to Atkinson [3], by keeping the diameter$(\Gamma) < 1$. In the absence of a proof of the uniqueness of the homogeneous cases of (2.8) and (2.9) in 2d on non-pathological boundaries, we will rely on numerical results. One expects that a singular BIE formulation will lead to a singular numerical approximation. Atkinson defines the condition number of Fredholm equation of the second kind as

$$cond(I + \lambda A) = \|I + \lambda A\|\|(I + \lambda A)^{-1}\|. \tag{2.33}$$

He then shows that the condition number for a singular equation is infinite. To identify whether or not this is the case for our operators, we will observe condition numbers of the linear system resulting from our discretization. Convergence of a solution is not alone evidence to the uniqueness of our formulation, since we could be computing a permissible non-unique solution for the given right hand side.

Alternative formulations for the Robin problem are given by Constanda in [5]. The first relies on knowing a-priori the unique function Φ for a given contour, making it less convenient for numerical calculations. He also identifies a direct method for solving the Robin problem that similarly requires a non-pathological boundary, though he states that this is unnecessary if β is a constant. He also mentions a possible adaptation for computations on a pathological boundary, though these also rely on some knowledge of the logarithmic capacity.

We also note that our exterior problem admits solutions with logarithmic growth at infinity for certain boundary conditions. While this is not consistent with our stated exterior problem, we note that Greenbaum et al. [1] mention that logarithmic growth in the far-field for their 2d Dirichlet problem is well posed and can be computed if desired. In our case, we restrict ourselves to appropriate boundary data yielding the proper far-field conditions. This is similar to invoking the compatibility constraints of the exterior Neumann problem in 2d. We also look to the condition numbers of the linear system of our numerical approximation to give evidence that the exterior formulation is a well formulated equation of the second kind.

Chapter 3

Numerical Treatment of Boundary Integral Equations

Having described the formulation of our integral equations and given an overview of some of the appropriate theory, we now turn to the numerical approximations used to construct fast numerical solutions to the Robin problem that have a high degree of accuracy. The primary difficulties in constructing highly accurate solutions to our integral equations is numerically resolving the singular nature of their kernels. Though their integral exists, pointwise evaluation done by straightforward integration rules cannot resolve the singularity. As a result, specialized techniques are required to integrate the singularity to high order. A secondary problem is representing the boundary surfaces and densities of the problem to high order accuracy. Both the 2d and 3d problems require differentiation and interpolation on surfaces in order to construct discrete measurements of geometric quantities such as curvature and sample values at quadrature points. This chapter will proceed by giving an overview of the core practices of our 2d numerical treatment of the Robin problem: Nyström's method and specialized quadratures. This overview of the 2d problem will be followed by a review of recently published methods that could be applied to the Robin problem in 3d.

3.1 Nyström's Method

The basis for our numerical treatment of integral equations for the Robin problem is called Nyström's method. Our integral equations can be conceptualized as being of the form

$$\sigma(x) + \int_\Gamma \mathbb{K}(x,y)\sigma(y)dy = g(x), \quad x, y \in \Gamma \tag{3.1}$$

with kernel $\mathbb{K}(x,y)$. Given a quadrature scheme with quadrature points y_i and weights w_i we can construct a semi-discretized version of (3.1)

$$\sigma(x) + \sum_{i=1}^{N} w_i \mathbb{K}(x,y_i)\sigma(y_i) = g(x). \tag{3.2}$$

A fully discretized system can be achieved by requiring (3.2) to hold at the quadrature points themselves:

$$\sigma(x_i) + \sum_{i=1}^{N} w_i \mathbb{K}(x_i,y_i)\sigma(y_i) = g(x_i). \tag{3.3}$$

Solving the linear system gives an approximation $\sigma(x_i)$ valued at the quadrature points. With this approximation we can in turn consider (3.2) as an interpolation formula for $\sigma(x)$ on Γ. This method of discretization and interpolation is known as Nyström's method and Nyström interpolation. In addition to giving the values on the boundary, for our purpose, the approximate σ can also be used with the same quadrature rules in the single layer potential (2.20) of the PDE solution:

$$u(x) = \sum_{i=1}^{N} w_i \sigma(y_i) G(x,y_i). \tag{3.4}$$

One of the advantages of the Nyström method is that it can be shown that in some cases the condition number of the linear system resulting from (3.3) can be bounded by the condition number of the integral operator [3]. In the case of Fredholm equations of the second kind, the condition number of the operator is bounded when the equation is uniquely solvable [3]. Our numerical results similarly exhibit the bounded behaviour of the condition numbers.

3.2 Numerical Treatment of the 2D Robin Problem

In this section we describe in detail our high-order Nyström's method implemented for numerically solving the BIEs (2.8) and (2.9). We note that we can write both the exterior and interior problems

as

$$-\beta\left[\sigma(x)/2 \pm \int_\Gamma \sigma(y)\frac{1}{2\pi}\partial_{nx}\log|y-x|dS_y\right] + \int_\Gamma \sigma(y)\frac{1}{2\pi}\log|y-x|dS_y = g(x). \tag{3.5}$$

To effectively apply Nyström's method we need to first construct the computational domain which are the curves comprising Γ. We then must use efficient quadrature rules that resolve the singular nature of the equations to high order accuracy.

In two dimensions, Γ is a single smooth closed curve for the interior problem and a set of non-overlapping smooth closed curves Γ_η for the exterior one as seen in Figure 2.1 . To get high-order accuracy we construct the $(\hat{x}, \hat{y})$ coordinates of these curves from a Fourier representation in the complex plane.

$$\Gamma_\eta(t) = \hat{x}_\eta(t) + i\hat{y}_\eta(t) = \sum_{k=-k_m}^{k_m} C_{k\eta}e^{ikt} \; 0 \le t < 2\pi. \tag{3.6}$$

Though any closed smooth curve can be represented by taking $k_m \to \infty$, we restrict ourselves to curves which are explicitly represented by finite k_m. This allows us to compute necessary geometric qualities of the curve exactly. This is particularly useful since the limit as $x \to y$ on Γ of $\partial_{n_x}\log|x-y|$ is $\kappa(y)/2$ where $\kappa(y)$ is the curvature of the boundary. We can compute the curvature from (3.6)

$$\hat{x}'(t) + i\hat{y}'(t) = \sum_{-k}^{k} ikC_k e^{ikt}, \tag{3.7}$$

$$\hat{x}''(t) + i\hat{y}''(t) = \sum_{-k}^{k} -k^2 C_k e^{ikt}, \tag{3.8}$$

$$\kappa(t) = \frac{\hat{x}'(t)\hat{y}''(t) - \hat{y}'(t)\hat{x}''(t)}{(\hat{x}'(t)^2 + \hat{y}'(t)^2)^{3/2}}. \tag{3.9}$$

We can also rewrite our integral equations in terms of the parameter t, considering only a single curve for the exterior problem.

$$\begin{aligned}-\beta(x(t))\left[\sigma(x(t))/2 \pm \int_0^{2\pi} \sigma(y(t))\frac{1}{2\pi}\partial_{nx}\log|y(t)-x(t)||y'(t)|dt\right] \\ + \int_0^{2\pi} \sigma(y(t))\frac{1}{2\pi}\log|y(t)-x(t)||y'(t)|dt = g(x(t)).\end{aligned} \tag{3.10}$$

Again, we can use the explicit form of Γ to construct the arclength $|y'(t)|$ using (3.7). We can now construct a numerical scheme based on Nyström's method using the trapezoid rule. For $dt = 2\pi/N$

and $t_i = i \cdot dt$ for $i, j = 1..N$, $x_i = x(t_i)$ and normal vector $n(x(t))$ and $r_{ji} = x_j - x_i$ we have the discrete system,

$$-\beta(x_i)\left[\sigma(x_i)/2 \pm dt\sum_{j=1}^{N}\sigma(x_j)\frac{1}{2\pi}\frac{n(x_i)\cdot r_{ji}}{|r_{ji}|}|x_j'|dt\right] + dt\sum_{j=1}^{N}\sigma(x_j)\frac{1}{2\pi}\log|r_{ji}||x_j'|dt = g(t_i). \tag{3.11}$$

This discretization yields a problem; In two of the terms above, we divide by $|r_{ii}| = 0$. In the Neumman component, we can substitute $\frac{n(x_i)\cdot r_{ii}}{|r_{ii}|} = \kappa(x(t_i))/2$. However, in the second Dirichlet component we must resolve the logarithmic singularity. To do so we use specialized quadrature rules constructed by Alpert [2] for computing logarithmic singularities with the trapezoid rule.

3.2.1 Hybrid Gauss-Trapezoidal Quadratures

The quadrature rules designed by Alpert are called hybrid Gauss-trapezoidal (HGT) quadrature rules. These rules integrate a function with a singularity at the end of an interval with high-order Gaussian quadrature rules, while utilizing the trapezoid rule on the interior. Alpert designed the quadratures to allow for the integration of singular integral operators while still allowing fast methods to be applied. The HGT rules take a trapezoidal rule on an interval and replaces a fixed number of equally spaced trapezoid quadrature points near the singular endpoints with different gaussian weights and points. Figure 3.1 shows the extra end points added to successively higher orders of the HGT rules. The internal points still maintain the equispaced nature of the trapezoid rule.

Rule 1	$O(h^2 \log(h))$	Rule 7	$O(h^{10} \log(h))$
Rule 3	$O(h^4 \log(h))$	Rule 8	$O(h^{12} \log(h))$
Rule 5	$O(h^6 \log(h))$	Rule 9	$O(h^{14} \log(h))$
Rule 6	$O(h^8 \log(h))$	Rule 10	$O(h^{16} \log(h))$

Table 3.1: Orders of convergence for hybrid Gauss-trapezoidal quadrature rules.

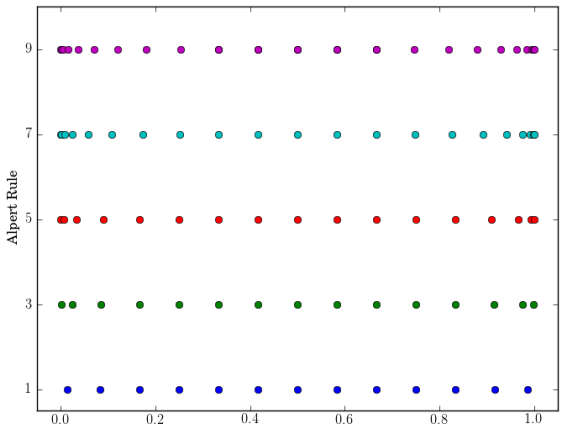

Figure 3.1: Hybrid Gauss-trapezoidal quadrature points.

Given a function of the form $g(x) = \phi(x)[(log(x) + log(1-x)]$ we have (HGT) quadrature rule:

$$\int_0^1 g(x)dx \approx h\sum_{i=1}^{j} u_i g(v_i h) + h\sum_{k=0}^{n-1} g(ah+kh) + h\sum_{i=1}^{j} u_i g(1-v_i h) \tag{3.12}$$

where h is the stepsize $h = 1/(2a+n)$, the nodes v_i and weights u_i are given in the appendix. We will refer to the nodes and weights v_i and u_i as hybrid nodes and weights. The orders of convergence for some of these quadrature rules are given in table 3.1 and their weights and quadrature nodes are given in the appendix. Figure 3.2 gives a numerical example of the convergence of the hybrid rules for the integral $\int_0^1 [\log(x) + \log(1-x)]\, dx$. The first five rules exhibit the corresponding orders of convergence. These quadrature rules are for the interval $[0, 1]$, however, they extend nicely to our contour integrals if we consider our closed boundary contour as beginning and ending at the singularity $x(t_i)$. In this case, the hybrid quadrature nodes replace a diagonal section of the

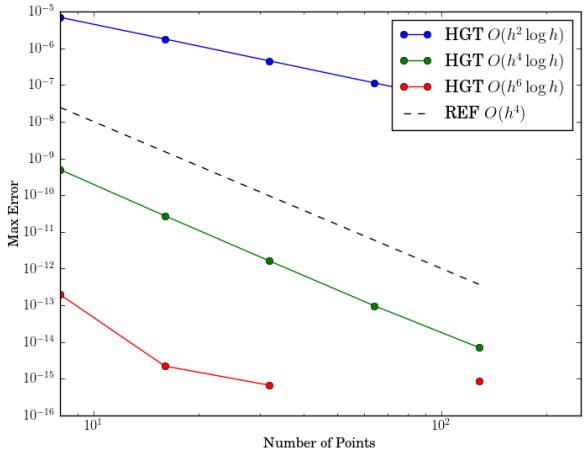

Figure 3.2: Convergence of HGT quadrature rules for $\int_0^1 [\log(x) + \log(1-x)]\, dx$.

Dirichlet operator matrix in (3.11) to integrate the singularity $\log(|r_{ii}|)$. One cannot simply fill in these diagonals, however. We have the problem that the discrete $\sigma(y_j)$ only has the values given at equally spaced points for the trapezoidal rule. In order to construct σ at the hybrid gauss-trapezoidal quadrature points, we need to interpolate σ around each singularity. We must do this to at least as high enough order as that of the order of convergence of the quadrature rules . To do so, we use a Fourier interpolation to compute σ at the hybrid quadrature points which is spectrally accurate. In the t parameter, each of the hybrid quadrature points for a single singularity has an equivalent point that is the same distance away from its respective singularity $\log(|r_{ii}|)$ as seen in Figure 3.3 . We can interpolate σ at each of these equi-distance points by phase-shifting the discrete Fourier transform of σ at the regular points then computing its inverse transform. This requires a complexity of $O(N \log(N))$ when using fast-Fourier methods to compute the interpolation.

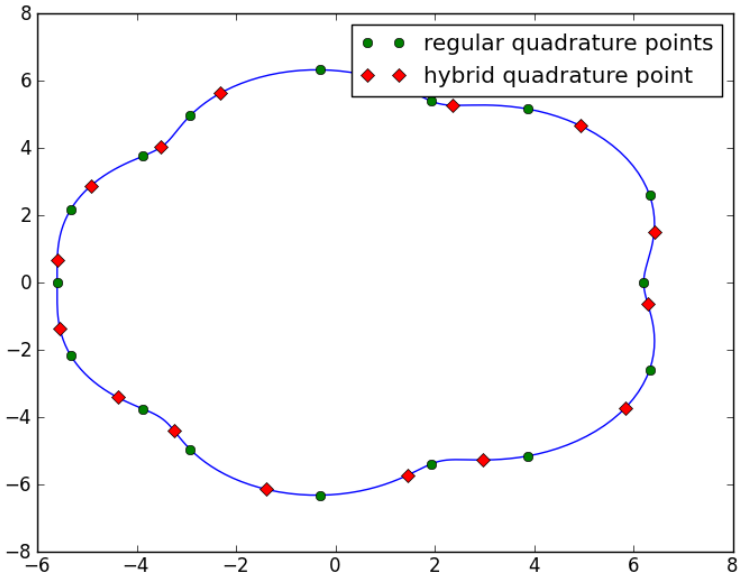

Figure 3.3: Equidistant hybrid quadrature points in parameter t from regular points.

The matrix corresponding to the process of interpolating $\sigma(y_j)$ and then computing the Alpert quadratures is never constructed. Instead, the process is implemented as a matrix-vector routine for an iterative linear solver which computes the numerical solutions.

Once $\sigma(y_j)$ is computed, u is computed by applying the trapezoid rule to the single layer potential (2.20).

3.3 Iterative Linear Solvers

Using a quadrature rule in (3.3) leads to a dense matrix system. Direct solvers such as Gaussian-elimination give a worst case $O(N^3)$. Iterative solvers and fast summation methods reduce this cost to $O(N)$ in some cases. A widely used iterative linear solver for integral equations is the Generalized Minimal Residual Method, known as GMRES. For linear systems resulting from the numerical treatment of integral equations of the second kind, GMRES can converge with a constant number of iterations, independent of the size of the linear system. We observe this in our numerical

experiments with the Robin Kernels. Since GMRES relies only on the vector-matrix product of the discretization matrix, the asymptotics of solving (3.3) are practically reduced to the $O(N^2)$ cost of the matrix-vector product. To reduce this cost further, fast summation methods can be used to calculate the matrix-vector product in $O(N \log N)$ or $O(N)$. An example of these methods are tree-codes and fast multipole methods. The combination of these two techniques, iterative solvers and fast multipole methods, are the basis for many modern integral equation methods.

3.4 The 3d problem: review of some recent techniques

Having described our 2d method for the Robin problem, we now provide a discussion on methods for computing the Robin problem in three dimensions. High order and fast algorithms for singular integral equations in three dimensions is a current topic of research. We will review the techniques used recently by Veerapaneni et al. in [9] for blood vesicle modelling and describe how they could be applied to our problem in three dimensions. [9] includes techniques for describing a surface to high-order in three dimensions, along methods to compute quadrature of weakly-singular kernels superalgebraically. Unfortunately, their specialized singular quadrature methods require a global interpolation for each quadrature point, which is comparatively more costly than the local interpolation used to compute HGT quadrature rules in our method.

3.4.1 High Order Surfaces in 3d

In order to construct high-order surfaces in three dimensions, Veerapanini et al. use an equivalent method as ours in 2d, representing their surface as a parameterization by a Fourier basis. In three dimensions, their Fourier basis is a triplet of spherical harmonics expansions, already introduced to us by 3d fast methods. Note that in this section, however, the spherical harmonics include the standard normalization and are defined as in [9]. In 3d, for a point $(\hat{x}(s,t), \hat{y}(s,t), \hat{z}(s,t))$ on Γ we have the parameterization

$$\begin{pmatrix} \hat{x}(s,t) \\ \hat{y}(s,t) \\ \hat{z}(s,t) \end{pmatrix} = \begin{pmatrix} \sum_{n=0}^{\infty} \sum_{m=-n}^{n} B_n^m Y_n^m(s,t) \\ \sum_{n=0}^{\infty} \sum_{m=-n}^{n} C_n^m Y_n^m(s,t) \\ \sum_{n=0}^{\infty} \sum_{m=-n}^{n} D_n^m Y_n^m(s,t) \end{pmatrix} \tag{3.13}$$

An example parameterization is

$$\begin{aligned} B_1^1 = i, \quad B_1^{-1} = 1 \\ C_1^1 = -i, \quad C_1^{-1} = 1 \\ D_1^0 = 1 \end{aligned} \tag{3.14}$$

which gives the parameterization for the surface of a unit sphere as seen in Figure 3.4. Given such

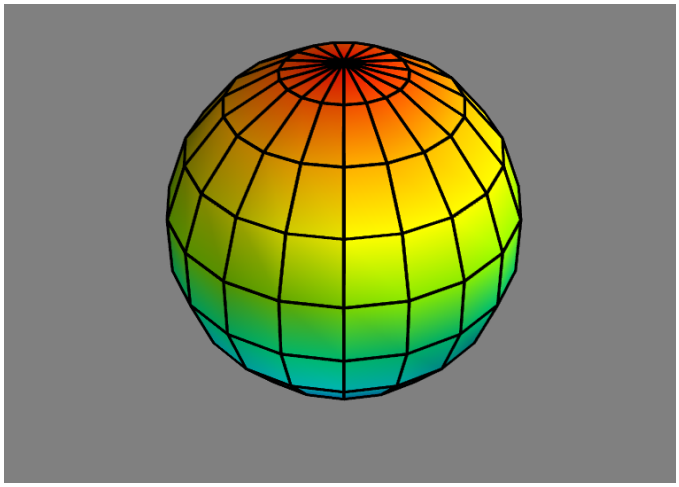

Figure 3.4: Sphere parameterization.

a representation of a surface, one can numerically integrate a function f on that surface first by discretizing $t_j = \{\cos^{-1}(p_j)\}$ where p_j are the $l+1$ Gauss-Legendre quadrature nodes on the interval $[-1, 1]$ with weights λ_j and $s_i = \{i\Delta s, \quad \Delta s = \frac{\pi}{2l+2}, i = 0..2l+1\}$ thus giving points $x_{ij} = [\hat{x}(s_i, t_j), \hat{y}(s_i, t_j), \hat{z}(s_i, t_j)]$ on Γ. The integral is then computed by the following quadrature rule:

$$\int_\Gamma f d\Gamma = \sum_{i=0}^{2l+1} \sum_{j=0}^{l} w_{ij} f(x_{ij}) A(x_{ij}). \tag{3.15}$$

Where A is the infinitesimal area computed from the surface representation and w_{ij} is the quadrature weights

$$w_{ij} = \frac{\pi}{l} \frac{\lambda_j}{\sin t_j}. \tag{3.16}$$

This quadrature converges superalgebraically for smooth f. If we considered using this quadrature to compute the discrete formulation of a boundary integral equation (3.3) this would require $O(l^4)$ operations for a single matrix-vector product. Alternatively if one could apply the fast-multipole method, the matrix vector product would be $O(l^2)$.

3.4.2 Singular Quadratures

In order to accurately integrate singular kernels, specialized quadratures are used by Veerapenini et al. Unfortunately, these quadrature rules are dependent on a global rotation and interpolation for every quadrature point. The technique depends on integrating a singularity at the point $t, s = 0, 0$, the effective "pole" of the parametrization. At this point, a function of the form $\frac{f(x)}{|x_{00}-x|}$ can be integrated superalgebraically with the quadrature rule

$$\int_\Gamma \frac{f(x)}{|x_{00}-x|} dS_x = \sum_{i=0}^{2l+1} \sum_{j=0}^{l} \frac{w_{ij}^s}{|x_{00}-x_{ij}|} f(x_{ij}) A(x_{ij}), \tag{3.17}$$

$$w_{ij}^s = w_{ij} \sum_{n=0}^{l} \frac{4\pi}{\sqrt{2(2n+1}} \frac{P_n(\cos(t_j))}{\cos(t_j/2)}. \tag{3.18}$$

Since the matrix-vector product of the form (3.3) is a convolution, a singularity must be integrated at each quadrature point, corresponding to a row sum of (3.3). The method of Veerapaneni to compute this singular integration is to first rotate the parameterization as seen in Figure 3.5 so that the pole is at the quadrature point. Computing the rotated parameterization requires computing rotation matrices; We used techniques described in [4] to create Figure 3.5. Unfortunately, on the rotated grid the quadrature points have changed globally. One must therefore globally interpolate σ to the new quadrature points. This is done by first transforming σ into a spherical harmonic expansion. This expansion is rotated similar to the surface parameterization. Then σ at the new points is interpolated by performing an inverse transform. The primary cost given by Veerapeneni for their method is due to the rotations at $O(l^3)$. The final asymptotic complexity of the matrix-vector product is $O(l^5)$. In addition, since the quadrature points are globally shifted for each row sum, it is not immediately apparent how one could construct a fast summation scheme to compute the matrix vector product. Even if one did, the asymptotic complexity of the scheme wouldn't be affected, at least for a single surface. Veerapenini et al. do effectively use fast methods when the domain is composed of many closed non-overlapping surfaces.

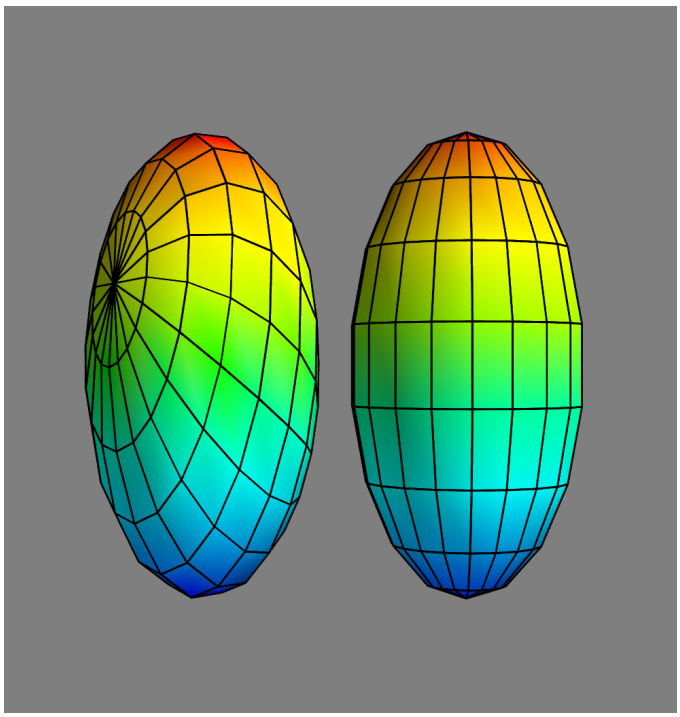

Figure 3.5: Rotated spherical harmonics parameterization of an ellipsoid.

Chapter 4

The Robin Problem in 2d: Results

This chapter contains the numerical results obtained from solving the Robin Problem on interior and exterior domains using a Nystroms method with HGT quadrature rules which we will refer to as the NHGT method. The sections in this chapter will cover the following results:

1. convergence studies for $\beta = 1$ for both the interior and exterior problem on simple and complex domains.
2. convergence studies on multiply-connected domains and problems with $\beta(x)$ varying over the contour.
3. condition numbers and observations of taking the limit of $\beta \to 0$
4. convergence of the first kind integral equation solving the Dirichlet problem corresponding to $\beta = 0$.

In all of our examples, we required GMRES to converge to a minimum residual of 10^{-12} with a restart at 20 iterations. Once the corresponding BIE is solved, we compute the solution of the Robin problem using the single layer potential (2.20). This is done using a trapezoid rule with the same number of quadrature points as was used to solve the BIE.

4.1 Convergence Studies for $\beta = 1$

We present here the results of our hybrid quadrature Nyström's method for the interior and exterior Robin problem for $\beta = 1$.

Figure 4.2 shows the absolute error convergence of the solution to the interior Robin problem. The computed solution is shown in Figure 4.1. The boundary Γ is an ellipse with semi-major axis $\frac{2}{5}$ and semi-minor axis $\frac{1}{5}$ the solution $u(\hat{x}, \hat{y}) = \hat{x}^2 - \hat{y}^2$ was used to create the appropriate boundary conditions and test for convergence. One can see that the numerical solution enjoys rapid convergence, especially for quadrature rules 5 and higher, which all converge essentially with $O(h^{10})$ until reaching round-off error. GMRES converged in 8 iterations, regardless of the number of discretization points.

Figure 4.4 shows the absolute error convergence of the solution to the exterior Robin problem. The computed solution is shown in Figure 4.3. The boundary Γ is the same as the previous interior problem. In this case, the exterior solution is given by the potential of two point charges, one with unit charge at $x = (0, 0)$ and one with a negative unit charge at $x = (.05, 0)$ so that the solution is $O(1/|x|)$ as $x \to \infty$. One can see that the numerical solution enjoys similar rapid convergence as the interior problem. In this exterior case, GMRES converged in 9 or less iterations.

Figure 4.6 shows the absolute error convergence of the solution to the interior Robin problem. The computed solution is shown in Figure 4.5. The boundary Γ is now much more complicated. The interior solution is still $\hat{x}^2 - \hat{y}^2$ with appropriate boundary conditions. In these tests, GMRES decreased from 33 to 23 iterations as the number of discretization points N increased.

Figure 4.8 shows the absolute error convergence of the solution to the exterior Robin problem. The computed solution is shown in Figure 4.7. In this case, the exterior solution is given by the potential of two point charges, one with unit charge at $x = (-1/10, 0)$ and one with a negative unit charge at $x = (-1/20, 0)$. In this exterior case, the number of iterations GMRES required looked to converge to 31 iterations as N increased, with 35 the highest iteration count.

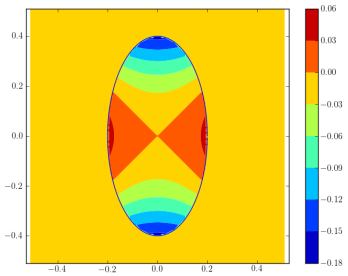

Figure 4.1: Numerical solution of the interior Robin problem, $\beta = 1.0$ with elliptic boundary.

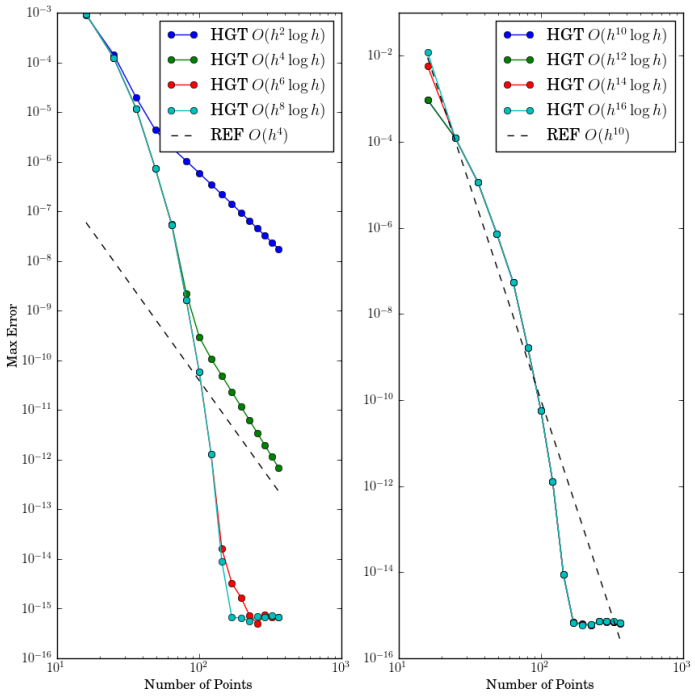

Figure 4.2: Convergence of the NHGT method. The legend identifies convergence rates using different orders of HGT quadrature rules. Reference lines (REF) show $O(h^4)$ convergence and $O(h^{10})$ convergence for comparison.

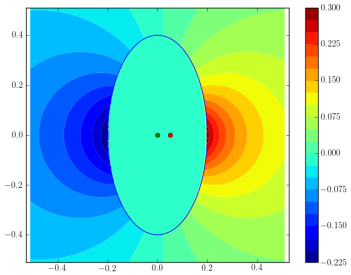

Figure 4.3: Numerical solution of the exterior Robin problem, $\beta = 1.0$ with elliptic boundary.

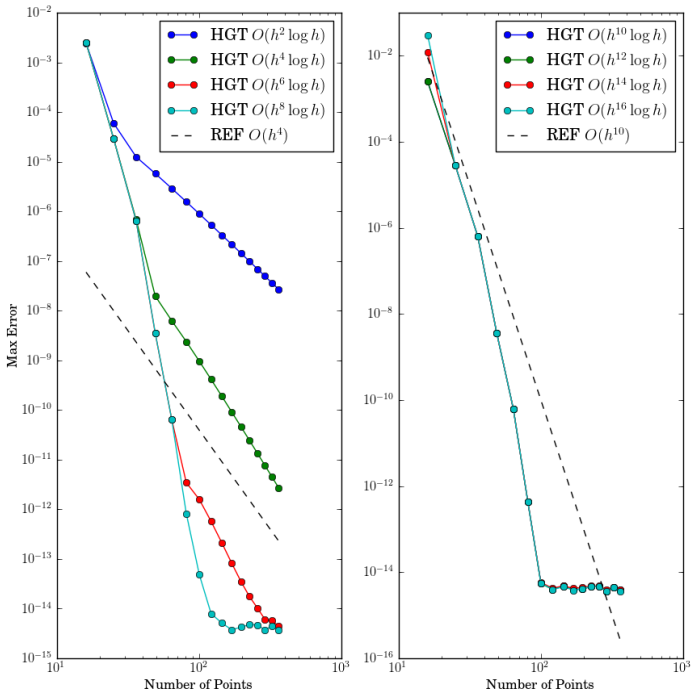

Figure 4.4: Convergence of the NHGT method. The legend identifies convergence rates using different orders of HGT quadrature rules. Reference lines (REF) show $O(h^4)$ convergence and $O(h^{10})$ convergence for comparison.

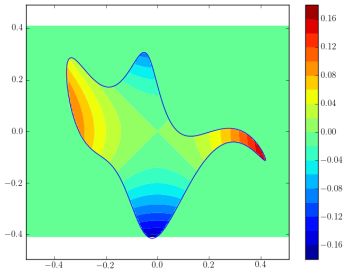

Figure 4.5: Computed solution of the interior Robin problem, $\beta = 1.0$ with complicated boundary.

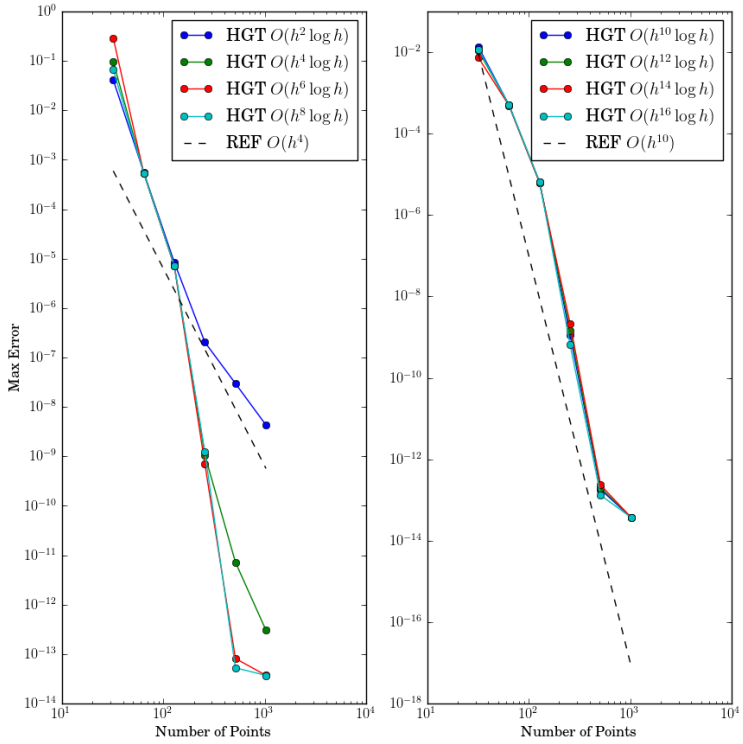

Figure 4.6: Convergence of the NHGT method at various HGT quadrature rule orders for the interior Robin problem, $\beta = 1.0$ with complicated boundary.

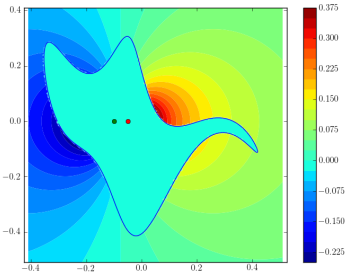

Figure 4.7: Numerical solution of the exterior Robin problem, $\beta = 1.0$ with complicated boundary.

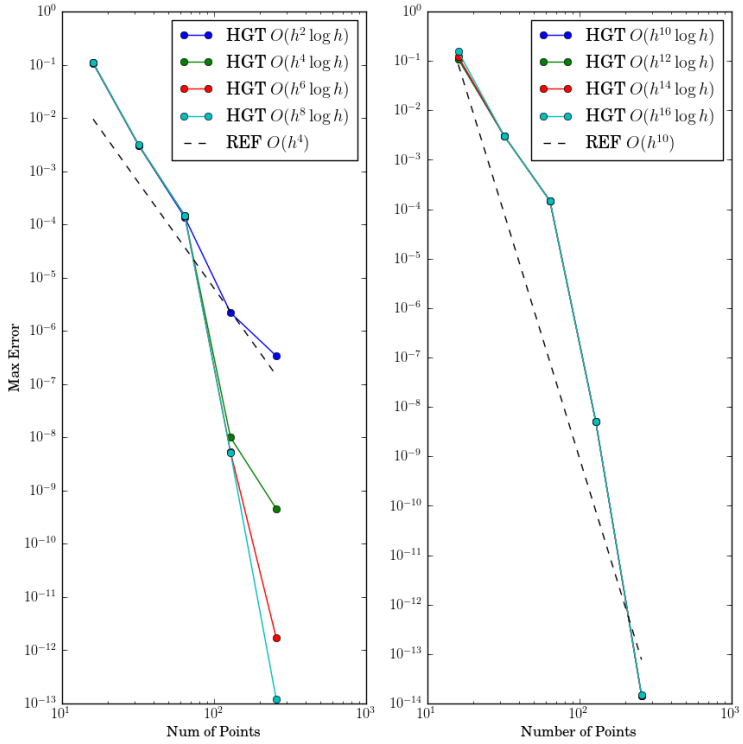

Figure 4.8: Convergence of the NHGT method at various HGT quadrature rule orders for the exterior Robin problem, $\beta = 1.0$ with complicated boundary.

4.2 Multiply-Connected Domains and $\beta(x)$ Varying over the Contour

In this section we study the convergence of the Robin method for multiply-connected domains in the exterior case and for cases where $\beta(x)$ varies over Γ.

Figure 4.10 shows the absolute error convergence of the solution to the exterior Robin problem, with Γ composed of three boundaries. The solution is shown in Figure 4.9. In this case, the exterior solution is given by the potential due to point charges in the interior of the boundaries; The two horizontal ellipses contain unit charge each at $x = (-4/10, 0)$ and $x = (0, 0)$. The lower circular boundary contains a point charge with charge -2 at $x = (-2/10, -4/10)$. In these calculations, the exterior Robin problem exhibited convergence of GMRES bounded by 12 iterations.

Figure 4.12 shows the absolute error convergence of the solution to the Robin problem with Γ composed of four boundaries. The solution is shown in Figure 4.11. In this case, the exterior solution is given by $u(\hat{x}, \hat{y}) = \hat{x}^2 - \hat{y}^2$. In these calculations, the interior Robin problem exhibited convergence of GMRES bounded by 30 iterations.

The following two figure sets compute the solutions on simple elliptic boundaries as in the previous section. However, we now let β vary over the boundary. For both exterior and interior cases we set $\beta(x) = 1 + \frac{\cos(t)}{2}$ where t is the $[0, 2\pi]$ parameter describing the contour.

Figure 4.13 shows the absolute error convergence of the solution to the interior Robin problem, with Γ the same ellipsoid. The solution is shown in Figure 4.1. This interior problem converged in a maximum of 21 GMRES iterations, regardless of the number of discretization points.

Figure 4.14 shows the absolute error convergence of the solution to the interior Robin problem, with Γ the same ellipsoid. The solution is shown in Figure 4.3. This exterior problem converged in a maximum of 22 GMRES iterations, regardless of the number of discretization points.

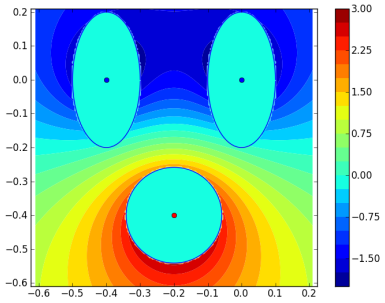

Figure 4.9: Numerical solution of the exterior Robin problem on a domain with multiple boundaries, $\beta = 1.0$.

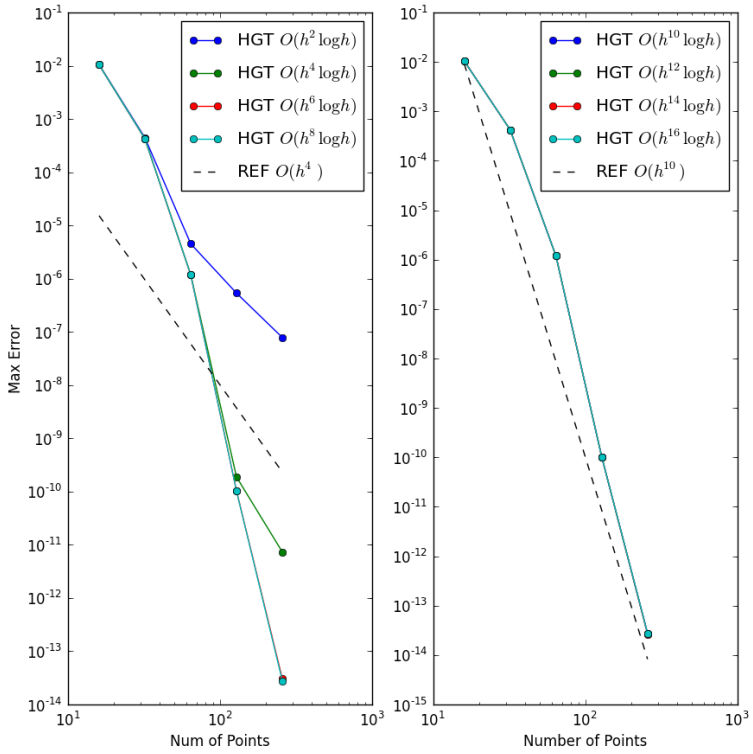

Figure 4.10: Convergence of the NHGT method for the exterior Robin problem on a domain with multiple boundaries, $\beta = 1.0$.

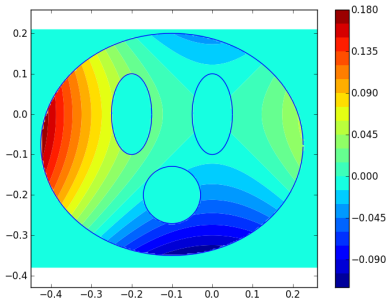

Figure 4.11: Numerical solution of the interior Robin problem on a bounded multiply connected domain, $\beta = 1.0$.

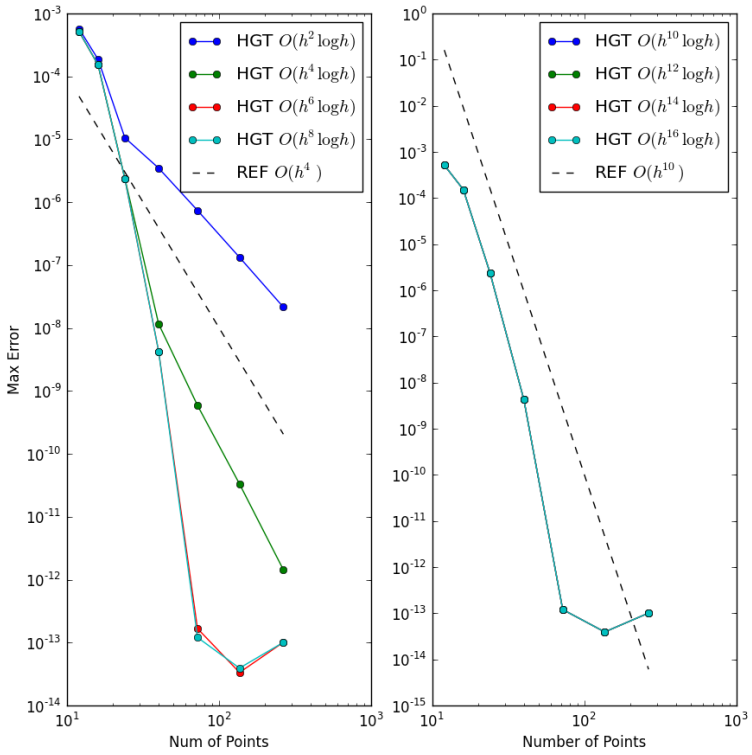

Figure 4.12: Convergence of the NHGT Method for the interior Robin problem on a bounded multiply connected domain, $\beta = 1.0$.

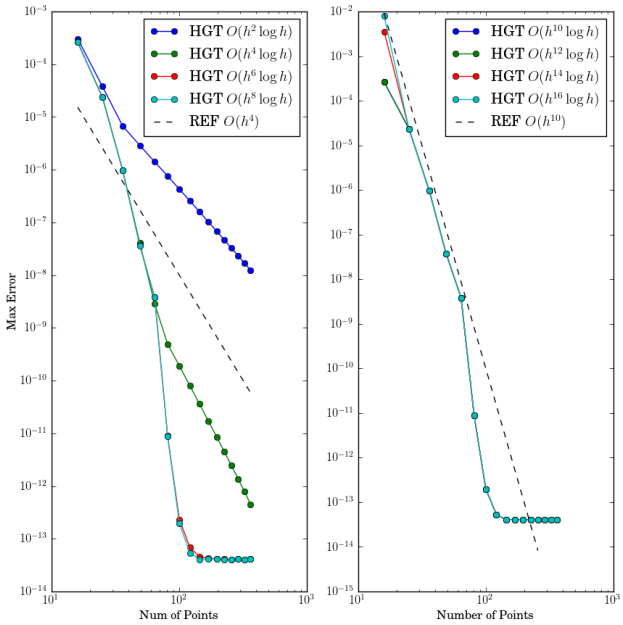

Figure 4.13: Convergence of the NHGT method for the interior Robin problem, $\beta = 1.0 + \frac{\cos(t)}{2}$.

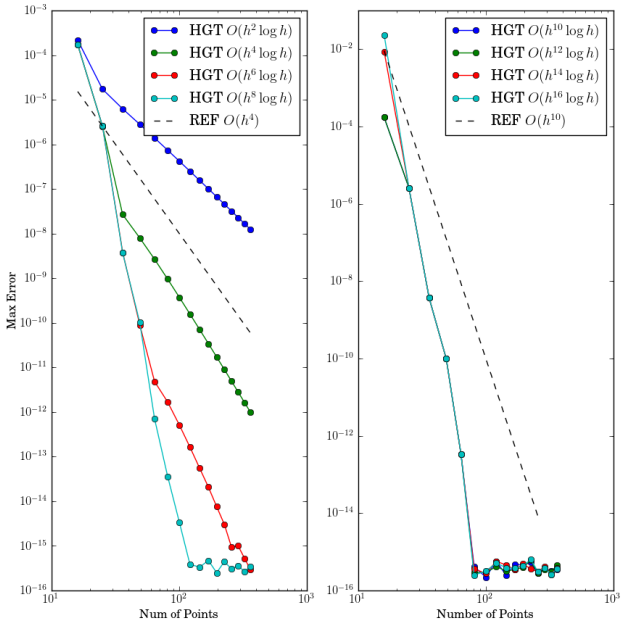

Figure 4.14: Convergence of the NHGT method for the exterior Robin problem, $\beta = 1.0 + \frac{\cos(t)}{2}$.

4.3 Condition numbers and the Near Dirichlet Limit

In this section we calculate condition numbers for our calculations. We are interested in experimenting with values of β at or approaching zero. We are particularly interested in finding the values of β for the condition numbers of the linear systems associated with numerical scheme should be bounded, similar to Atkinson's theorem in [3] that we mentioned in section 3.1. In addition, low condition numbers provide numerical evidence that our integral formulation of the second kind satisfies the Fredholm alternative with only a trivial null-space. One would expect a formulation with non-trivial null space to yield a singular matrix when using a consistent numerical approximation.

In computing the numerical solutions, we never explicitly create these linear systems due to the interpolation component of the hybrid quadrature scheme. To compute the condition number, we reconstruct the discretization matrix by computing the matrix-vector products on successive unit vectors of the form

$$V_i(j) = \begin{cases} 0 & i \neq j \\ 1 & i = j \end{cases} \tag{4.1}$$

Computing the matrix vector product on V_i allows us to recreate the i^{th} column of the matrix being solved in our method. The condition number is then computed using standard numerical routines.

Figure 4.15 shows the condition numbers corresponding to taking constant $\beta \to 0$ for the simple interior solution on the geometry and solution shown in Figure 4.1. For $\beta = 1$ we have the expected bounded conditioning of the system, but as β approaches zero, the conditioning has a sublinear growth that eventually approaches the linear growth in the condition number for $\beta = 0$. These calculations were done for Alpert rule 6. Surprisingly, even with $\beta = 0$, the numerical solution converges to the right answer. We will consider this case more in depth in the next section.

Figure 4.16 gives the condition numbers for the exterior geometry and solution shown in Figure 4.3. In the limit, the simple exterior problem exhibits similar behaviour as the interior one. Both of the $\beta = 1$ tests show a bounded condition number , consistent with Atkinson's theorem and with a well-conditioned integral equation formulation.

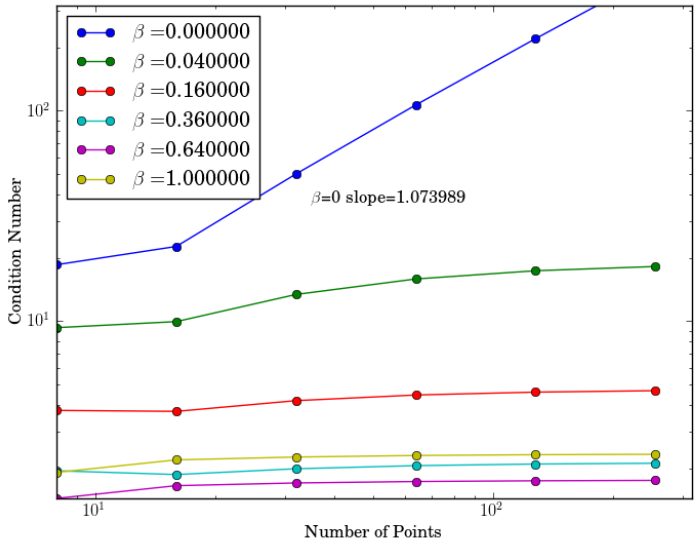

Figure 4.15: Condition numbers of the linear system resulting from the NHGT method for the interior Robin problem for various β.

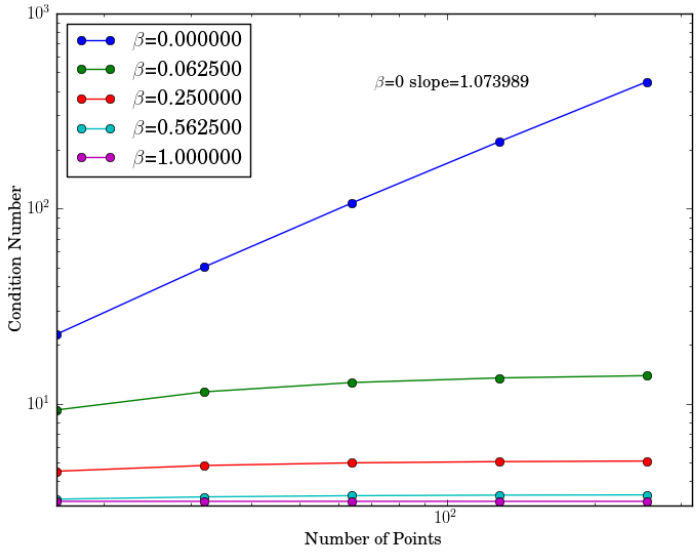

Figure 4.16: Condition Numbers of the linear system resulting from the NHGT method for the exterior Robin problem for various β.

4.4 The Dirichlet Problem and Integral Equations of the First Kind

Fredholm Integral equations of the first kind have historically been considered as an inappropriate way to construct numerical solutions to partial differential equations because numerical schemes based on such equations 'tend' to be ill-conditioned. However, when solving the integral equation of the first kind by applying the Robin method with $\beta = 0$, we have found that our numerical results converge. Though the conditioning of our problem grows linearly, solving the discretized method still exhibits a similar bound on the number of GMRES solutions for simple test geometry.

Taking $\beta = 0$ corresponds to solving the Dirichlet problem.

$$\nabla^2 u(x) = 0, \quad x \in \Omega, \tag{4.2}$$

$$u(y) = g(y), \quad y \in \Gamma. \tag{4.3}$$

We consider the same interior domain Ω and smooth boundary Γ as stated for the Robin problem. A particular solution to the Dirichlet problem can be sought by defining u by the single layer potential for density $\sigma(y), y \in \Gamma$

$$u(x) = \frac{1}{2\pi} \int_\Gamma \log|y - x| \sigma(y) dS_y, \quad x \in \Omega. \tag{4.4}$$

As described in Chapter two, the boundary conditions yield a Fredholm equation of the first kind

$$\frac{1}{2\pi} \int_\Gamma \log|y - x| \sigma(y) ds = f(x), \quad x \in \Gamma. \tag{4.5}$$

where Γ is a curve in $\mathbb{R}^2$. This the same equation as taking $\beta = 0$ for our Robin method. Figures 4.18 and 4.17 show the convergence and numerical solutions to the Dirichlet problem given the harmonic function

$$u(\hat{x}, \hat{y}) = e^{\hat{x}} \cos(\hat{y}), \tag{4.6}$$

and appropriate boundary data on the ellipse

$$\Gamma(t) = (\cos(t), 0.4 \sin(t)), \quad -\pi \leq t \leq \pi. \tag{4.7}$$

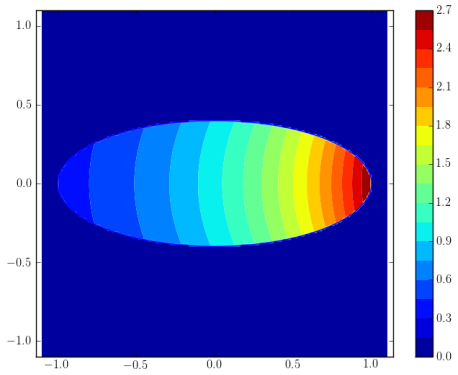

Figure 4.17: Computed solution of the Dirichlet problem with elliptic boundary.

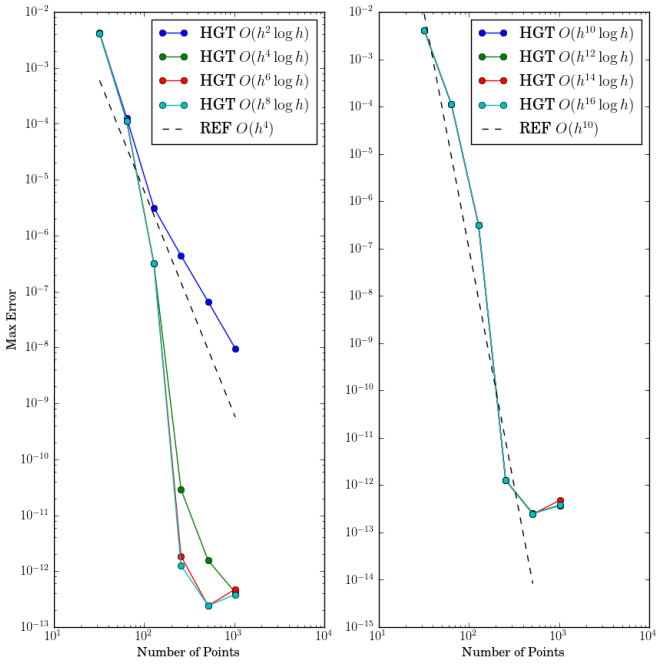

Figure 4.18: Convergence of the NHGT Method for the Dirichlet problem with elliptic boundary

In his book 'The Numerical Solution of Integral Equations'[3], Atkinson clarifies the ill-conditioned nature of integral equations of the first kind. He states that integral equations of the first kind with smooth kernels are ill-conditioned in that a small change in the boundary data yields large changes in the solution. However, for equation with singular kernels the conditioning is manageable. To investigate the effect of the condition number on our solution, we compute solutions to the above problem to a high number of quadrature points. This is to detect whether or not the conditioning of the system affects the numerical solution to the first kind equation. Tables 4.1,4.2, and 4.3 give maximum error of numerical solutions to (4.6) solved using our NHGT method. The numerical solution is computed with m quadrature points and given at the interior points $\alpha \cdot (\frac{1}{\sqrt{2}}, \frac{.4}{\sqrt{2}})$ with $\alpha = [0, .4, .8, .99]$. If we presume the linear growth in the condition matrix as shown in Figure 4.15, we might expect for $m = 10000$ to lose five digits of accuracy in our solution. Of course, this is only an upper bound on our error. Our actual convergence is much better. With GMRES solving to a minimum residual of 10^{-12} we are still able to resolve $\alpha = .99$ to 10^{-12} with 10000 quadrature points. Atkinson solves the same problem on the same geometry and our results can be compared with his. He solves the problem in the Fourier domain, where it becomes a Fredholm Equation of the second kind. Solving the first-kind equation directly means we lack the ability to discuss the uniqueness or existence of general solutions in context of the Fredholm alternative. However the high-order convergence of our method at least demonstrates the effectiveness of the HGT rules in numerically resolving the $\log$ singularities of our integral equations.

m \α	0	.4	.8	.99
20	-2.6e-05	-3.88e-04	-1.57e-02	1.3e-01
40	-2.25e-08	-5.62e-07	-6.53e-04	-1.11e-01
160	-6.84e-12	-1.18e-11	-6.13e-11	-2.25e-03
640	-5.11e-15	4.95e-14	1.93e-13	5.73e-06
1200	-7.11e-15	3.51e-14	-2.42e-13	7.02e-07
10000	2.78e-15	-4.44e-15	1.15e-13	-1.1e-12

Table 4.1: Errors for hybrid Gauss trapezoidal rule 4

m \α	0	.4	.8	.99
20	-2.8e-05	-3.71e-04	-1.57e-02	1.3e-01
40	-5.23e-09	-5.02e-07	-6.52e-04	-1.11e-01
160	4.44e-16	-3.55e-15	-5.8e-11	-2.25e-03
640	-2.22e-16	-2.22e-15	3.55e-14	5.73e-06
1200	-6.66e-16	-7.99e-15	8.99e-14	7.02e-07
10000	-4e-15	1.49e-14	-7.37e-14	-2.79e-13

Table 4.2: Errors for hybrid Gauss trapezoidal rule 7

m \α	0	.4	.8	.99
20	-2.23e-05	-3.67e-04	-1.57e-02	1.3e-01
40	-5.38e-09	-5.02e-07	-6.52e-04	-1.11e-01
160	-8.22e-15	4.49e-14	-5.83e-11	-2.25e-03
640	1.11e-15	-4.88e-15	3.73e-14	5.73e-06
1200	-8.88e-15	3.33e-14	-2.55e-13	7.02e-07
10000	3.66e-15	-7.55e-15	1.18e-13	-1.13e-12

Table 4.3: Errors for hybrid Gauss trapezoidal rule 10

Chapter 5

Conclusion

In this thesis we have investigated a boundary representation that gives rise to Fredholm equations of the second kind for exterior and interior domains for solving Laplace's equation with Robin boundary conditions. The equations have singular kernels for which we use specialized quadrature rules. We presented numerical results demonstrating high order convergence for our method on exterior, interior and multiply connected domains. We also presented results showing bounded condition numbers of our system when solving boundary conditions of the Robin type, giving evidence to a well-conditioned formulation. We observed condition numbers in the limit as our equations approached a Dirichlet boundary condition. Finally, we applied our singular quadrature methods directly to the Dirichlet problem, showing our method can converge to high-order despite the fact that the condition number of the numerical scheme grows unbounded as the number of quadrature points increases.

5.1 Future Work

While our results have been two dimensional, in Chapter 3 we discussed techniques that could be used to create numerical methods for three dimensions. Future work would include implementing our formulation for the Robin problem in three dimension using Veerapenini et al.'s techniques. In addition, researching more effective ways for integrating singular quadratures that are amenable to the fast summation methods would be an interesting direction.

The well-conditioned results of our numerics suggests one could try to prove that our integral formulations are well-conditioned and that solutions are unique and exist by the Fredholm Alternative. We suspect that for Γ not a pathological contour, one could prove this for our formulations of the interior problem and for the exterior problem if we allow logarithmic growth in the far field. One could also apply HGT quadratures to alternative integral equation formulations of the Robin problem given by Constanda in [5]

Appendix A

Hybrid gauss-trapezoidal rules

The following tables give the quadrature rules of order $O(h^l \log h)$, $h = 1/(2a + n)$

$$\int_0^1 g(x)dx \approx h\sum_{i=1}^{j} u_i g(v_i h) + h\sum_{k=0}^{n-1} g(ah + kh) + h\sum_{i=1}^{j} u_i g(1 - v_i h) \tag{A.1}$$

developed by Alpert [2] for integrating functions of the form $g(x) = \phi(x)[\log(x) + \log(1 - x)]$ for smooth ϕ.

rule	l	a	v_i	u_i
1	2	1	1.591549430918953d-1	5.0d-1
2	3	2	1.150395811972836d-1	3.913373788753340d-1
			9.365464527949632d-1	1.108662621124666d0
3	4	2	2.379647284118974d-2	8.795942675593887d-2
			2.935370741501914d-1	4.989017152913699d-1
			1.023715124251890d0	9.131388579526912d-1
4	5	3	2.339013027203800d-2	8.609736556158105d-2
			2.854764931311984d-1	4.847019685417959d-1
			1.005403327220700d0	9.152988869123725d-1
			1.994970303994294d0	1.013901778984250d0
5	6	3	4.004884194926570d-3	1.671879691147102d-2
			7.745655373336686d-2	1.636958371447360d-1
			3.972849993523248d-1	4.981856569770637d-1
			1.075673352915104d0	8.372266245578912d-1
			2.003796927111872d0	9.841730844088381d-1

rule	l	a	v_i	u_i
6	8	5	6.531815708567918d-3	2.462194198995203d-2
			9.086744584657729d-2	1.701315866854178d-1
			3.967966533375878d-1	4.609256358650077d-1
			1.027856640525646d0	7.947291148621894d-1
			1.945288592909266d0	1.008710414337933d0
			2.980147933889640d0	1.036093649726216d0
			3.998861349951123d0	1.004787656533285d0
7	10	6	1.175089381227308d-3	4.560746882084207d-3
			1.877034129831289d-2	3.810606322384757d-2
			9.686468391426860d-2	1.293864997289512d-1
			3.004818668002884d-1	2.884360381408835d-1
			6.901331557173356d-1	4.958111914344961d-1
			1.293695738083659d0	7.077154600594529d-1
			2.090187729798780d0	8.741924365285083d-1
			3.016719313149212d0	9.661361986515218d-1
			4.001369747872486d0	9.957887866078700d-1
			5.000025661793423d0	9.998665787423845d-1
8	12	7	1.674223682668368d-3	6.364190780720557d-3
			2.441110095009738d-2	4.723964143287529d-2
			1.153851297429517d-1	1.450891158385963d-1
			3.345898490480388d-1	3.021659470785897d-1
			7.329740531807683d-1	4.984270739715340d-1
			1.332305048525433d0	6.971213795176096d-1
			2.114358752325948d0	8.577295622757315d-1
			3.026084549655318d0	9.544136554351155d-1
			4.003166301292590d0	9.919938052776484d-1
			5.000141170055870d0	9.994621875822987d-1
			6.000001002441859d0	9.999934408092805d-1
9	14	9	9.305182368545380d-4	3.545060644780164d-3
			1.373832458434617d-2	2.681514031576498d-2
			6.630752760779359d-2	8.504092035093420d-2
			1.979971397622003d-1	1.854526216643691d-1
			4.504313503816532d-1	3.251724374883192d-1
			8.571888631101634d-1	4.911553747260108d-1
			1.434505229617112d0	6.622933417369036d-1
			2.175177834137754d0	8.137254578840510d-1
			3.047955068386372d0	9.235595514944174d-1
			4.004974906813428d0	9.821609923744658d-1
			4.998525901820967d0	1.000047394596121d0
			5.999523015116678d0	1.000909336693954d0
			6.999963617883990d0	1.000119534283784d0
			7.999999488130134d0	1.000002835746089d0

rule	l	a	v_i	u_i
10	16	10	8.371529832014113d-4	3.190919086626234d-3
			1.239382725542637d-2	2.423621380426338d-2
			6.009290785739468d-2	7.740135521653088d-2
			1.805991249601928d-1	1.704889420286369d-1
			4.142832599028031d-1	3.029123478511309d-1
			7.964747731112430d-1	4.652220834914617d-1
			1.348993882467059d0	6.401489637096768d-1
			2.073471660264395d0	8.051212946181061d-1
			2.947904939031494d0	9.362411945698647d-1
			3.928129252248612d0	1.014359775369075d0
			4.957203086563112d0	1.035167721053657d0
			5.986360113977494d0	1.020308624984610d0
			6.997957704791519d0	1.004798397441514d0
			7.999888757524622d0	1.000395017352309d0
			8.999998754306120d0	1.000007149422537d0

Bibliography

[1] Greenbaum A., L. Greengard, and McFadden G. B., *Laplace's Equation and the Dirichlet-Neumann Map in Multiply Connected Domains*, Journal of Computational Physics **105** (1993), no. 2, 267–348.

[2] B. K. Alpert, *Hybrid Gauss-Trapezoidal Quadrature Rules*, SIAM Journal on Scientific Computing **20** (1999), 1551–1584.

[3] Atkinson,K. E., *The Numerical Solution of Integral Equations of the Second Kind*, Cambridge Univ. Pr., 1997.

[4] C.H. Choi, J. Ivanic, M.S. Gordon, and K. Ruedenberg, *Rapid and stable determination of rotation matrices between spherical harmonics by direct recursion*, The Journal of Chemical Physics **111** (1999), 8825.

[5] C. Constanda, *Direct and indirect boundary integral equation methods*, Chapman & Hall/CRC, 2000.

[6] Kellog O. D., *Foundations of Potential Theory*, Dover Publications,inc, 1953.

[7] Folland,G. B., *Introduction to Partial Differential Equations*, Princeton Univ. Pr., 1995.

[8] S.G. Mikhlin, *Integral Equations*, Pergamon Press Ltd., 1957.

[9] S. K. Veerapaneni, A. Rahimian, G. Biros, and D. Zorin, *A fast algorithm for simulating vesicle flows in three dimensions*, Journal of Computational Physics **230** (2011), no. 14, 5610–5634.